

# **Fabrication and Properties of Nanocapacitors and Nanostructures prepared by Nanosphere Lithography**

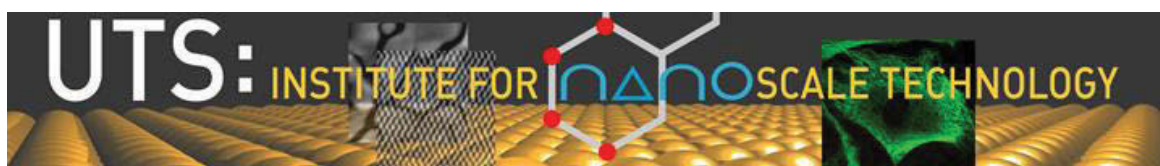
**by**

**Michael Coutts**

**Submitted for the Degree of  
Doctor of Philosophy**

**2016**

**University of Technology Sydney**



## **Certificate of Original Authorship**

I certify that the work in this thesis has not previously been submitted for a degree, nor has it been submitted as a part of requirements for a degree except as fully acknowledged within the text.

I also certify that the dissertation has been written by me. Any help that I have received in my research work and the preparation of the dissertation has been acknowledged. In addition, I certify that all information sources and literature used are indicated in the dissertation.

Michael Coutts

---

Date:

## Acknowledgements

First and foremost, I would like to thank my primary supervisor Assoc Prof Andrew McDonagh, the most patient person I know. I cannot thank you enough for your knowledge and guidance throughout the years.

Also special thanks to my co-supervisors Prof Mike Cortie and Dr Hadi Zareie. The depth of Mike's knowledge and enthusiasm of Hadi have helped me greatly.

For experimental assistance I would like to thank Dr Ric Wuhler (UWS), Mr Jean-Pierre Guerbois, Dr Ronald Shimmon, Dr Mark Berkahn, Dr Dylan Riessen, Dr Cuong Ton-That, Mr Geoff McCredie, Prof Matthew Phillips, Dr Tristan Rawling, Ms Katie McBean, Dr Angus Gentle, Dr Brian Reedy, Dr Matthew Arnold, Dr Annette Dowd, A/Prof Vicki Keast and A/Prof Mike Ford.

For support and encouragement thanks go to fellow postgraduate students Dr Nadine Harris, Dr Johnathan Edgar, Dr Marty Blaber, Dr Dakrong Pissuwan, Dr Nick Stokes, Mr Sylvan Rudduck, Dr Burak Cankurtaran, Dr Christine Austin, and Dr Amir Moezzi.

Thanks also goes to the assessors of this thesis, your feedback is greatly appreciated.

Finally, for financial support the Australian Research Council (DP0877539, DP0984354) and the University of Technology Sydney is acknowledged.

## Table of Contents

<i>Certificate of Original Authorship .....</i>	<i>ii</i>
<i>Acknowledgements .....</i>	<i>iii</i>
<i>Table of Contents .....</i>	<i>iv</i>
<i>List of Figures .....</i>	<i>viii</i>
<i>List of Tables .....</i>	<i>xxii</i>
<i>Abbreviations .....</i>	<i>xxiii</i>
<i>Publications and Conference Proceedings Arising From This Work.....</i>	<i>xxvi</i>
<i>Abstract .....</i>	<i>xxvii</i>
<b>1 Introduction.....</b>	<b>2</b>
<b>1-1 Thesis overview .....</b>	<b>2</b>
<b>1-2 Capacitors.....</b>	<b>2</b>
1-2.1 The evolution of Capacitors - A Brief History .....	4
1-2.2 Ideal Capacitance at the Nanoscale .....	8
1-2.3 Methods to Measure Nanoscale Capacitance .....	9
1-2.4 Materials for Nanoscale Capacitors .....	14
Metal Oxides .....	14
Metal Nitrides.....	16
Carbon Nanotubes .....	17
Graphene.....	21
Biological Nanocapacitors .....	24
Conducting Polymers .....	25
Other Materials .....	28
Monolayer-Protected Clusters .....	28
Metal Carbonyl Clusters .....	32
1-2.5 Applications of Nanoscale Capacitors.....	34
1-2.6 Summary and Outlook .....	34
<b>1-3 Project Aims .....</b>	<b>36</b>
<b>2 Experimental Section .....</b>	<b>38</b>
<b>2-1 Techniques Used In This Project .....</b>	<b>38</b>

2-1.1	Physical Vapour Deposition (PVD) .....	38
	Thin Film Growth .....	38
	Evaporative Deposition .....	39
	Sputter Deposition .....	40
2-1.2	Scanning Electron Microscopy (SEM) .....	41
2-1.3	Energy-Dispersive X-ray Spectroscopy (EDS) .....	42
2-1.4	Atomic Force Microscopy (AFM).....	44
<b>2-2</b>	<b>Experimental Details.....</b>	<b>45</b>
2-2.1	Materials Fabrication .....	46
	General .....	46
	Substrate Preparation .....	46
	Spin-Coating .....	46
	Lift-Off Method .....	47
	Gold Deposition.....	47
	Metal Oxide Deposition.....	47
	Film Thickness Monitor Calibrations .....	48
	Latex Sphere Removal .....	49
	Vacuum annealing experiments.....	50
	Zinc Oxide Growth Experiments.....	50
2-2.2	Characterisation .....	50
	SEM Experiments .....	50
	SEM Metrology.....	50
	AFM Measurements .....	50
	Monte Carlo Simulations.....	51
	Fitting of Grey-Scale Data.....	51
	EDS Measurements .....	51
	Cathodoluminescence Experiments.....	51
<b>3</b>	<b><i>Formation of Periodic Arrays using Nanosphere Lithography.....</i></b>	<b>53</b>
<b>3-1</b>	<b>Introduction .....</b>	<b>53</b>
<b>3-2</b>	<b>Results and Discussion .....</b>	<b>56</b>
3-2.1	Effect of spin-coat volume .....	56
3-2.2	Effect of Triton-X - methanol mixture concentration .....	58
3-2.3	Effect of Spheres Size On hcp Domain Size and Reproducibility .....	63
3-2.4	Effect of sonication time on the removal of the NSL mask.....	67
3-2.5	The Lift-Off Method as an Alternative for Mask Formation .....	69
3-2.6	Effect of Metal Deposition Techniques on Nanostructure .....	71

<b>3-3</b>	<b>Conclusions .....</b>	<b>74</b>
<b>4</b>	<b><i>SEM Charging of Gold-Metal Oxide-Gold Capacitors Synthesised by NSL* ..</i></b>	<b>77</b>
<b>4-1</b>	<b>Introduction .....</b>	<b>77</b>
<b>4-2</b>	<b>Results and Discussion .....</b>	<b>79</b>
4-2.1	Fabrication of multi-layer metal / metal oxide / metal nanostructure arrays.....	79
4-2.2	SEM imaging of multi-layer metal / metal oxide / metal nanostructure arrays .....	82
	Aluminium oxide as dielectric material .....	83
	Silicon dioxide as dielectric material .....	92
	Zinc oxide as dielectric material .....	95
	Titanium dioxide as dielectric material .....	99
	Hafnium dioxide as dielectric material.....	103
4-2.3	Comparison of different dielectric materials .....	107
4-2.4	Other experiments/observations.....	108
	Nanostructures with no dielectric material .....	108
	Substrate only measurements .....	112
	Retention of charge .....	119
	Sputter deposition and charging experiments .....	121
	Carbon minimisation on samples .....	122
<b>4-3</b>	<b>Conclusions .....</b>	<b>124</b>
<b>5</b>	<b><i>Templated Zinc Oxide Structures Grown from Salt Solution .....</i></b>	<b>126</b>
<b>5-1</b>	<b>Introduction .....</b>	<b>126</b>
<b>5-2</b>	<b>Results and Discussion .....</b>	<b>127</b>
5-2.1	Fabrication and structural characterisation of zinc oxide structures .....	127
	Characterisation by SEM .....	127
	AFM Characterisation.....	130
	EDS Characterisation .....	130
	Re-Emission in thin film deposition .....	133
5-2.2	Mechanism of zinc oxide structure formation.....	134
	Proposed mechanism .....	134
	Effect of surface composition on ring formation .....	136
5-2.3	Templates for hydrothermal growth of new zinc oxide structures .....	142
	Effect of template composition.....	143
	Effect of solution concentration.....	145
	Evolution of solution growth during incubation .....	146

Effect of incubation temperature.....	146
Effect of an applied potential.....	148
Cathodoluminescence experiments.....	149
<b>5-3 Conclusions .....</b>	<b>150</b>
<b>6 General conclusions .....</b>	<b>153</b>
<b>6-1 General discussions and conclusions.....</b>	<b>153</b>
<b>6-2 Future directions.....</b>	<b>154</b>
6-2.1 Nanosphere Lithography .....	154
6-2.2 SEM charging of nanoscale capacitors.....	155
6-2.3 Re-emission of Zinc Oxide and Solution Growth Experiments .....	159
<b>Appendix.....</b>	<b>161</b>
<b>7 Gold Nanoparticles for Charge Transport .....</b>	<b>161</b>
<b>7-1 Introduction .....</b>	<b>161</b>
<b>7-2 Experimental Methods.....</b>	<b>162</b>
7-2.1 Techniques Used In This Work.....	162
Thermal Gravimetric Analysis / Differential Scanning Calorimetry.....	162
Mass Spectrometry .....	164
X-Ray Photoelectron Spectroscopy .....	164
7-2.2 Experimental details .....	164
General.....	164
Synthesis of Gold Nanoparticles.....	165
Mass spectrometry and Thermal Analysis. ....	165
Synchrotron XPS Experiments. ....	166
<b>7-3 Results and discussion.....</b>	<b>166</b>
<b>7-4 Conclusions .....</b>	<b>172</b>
<b>References.....</b>	<b>174</b>

## List of Figures

Figure 1-1. (a) Illustration representing electrical discharge of a Leyden jar through the body. Image adapted from [6]. (b) Schematic of a Leyden jar. ....	4
Figure 1-2. Schematics representing the charging of two parallel plates by different potentials. ....	6
Figure 1-3. Schematic of double-layer capacitance. ....	7
Figure 1-4. DPV (dashed lines) and CV (solid lines) curves for hexanethiolate ligand monolayer protected clusters (MPCs). DPV highlights the peaks in the CV curve attributed to quantised electron double-layer charging. Curves adapted from [35]. ....	12
Figure 1-5. Nanoprobing to characterise the electrical properties of devices. (a) SEM micrograph of nanomanipulators making point contacts with a device. Image adapted from [44]. (b) AFM image of terminal contacts of a device which was electrically characterised by three CAFM tips making point contacts simultaneously (represented by schematic overlay). Image adapted from [45]. ....	13
Figure 1-6. Cyclic Voltametric curve of $\text{RuO}_2 \cdot x\text{H}_2\text{O}$ [57]. ....	14
Figure 1-7. Power density vs. Energy density for carbon nanotube and graphene based capacitors. Data has been extracted from reported values. ....	24
Figure 1-8. Schematic representation of the nanocapacitors studied by Barrientos <i>et al.</i> [246]. ....	25
Figure 1-9. Cyclic Voltammetric curve for the polypyrrole/polyaniline copolymer .....	26
Figure 1-10. Schematic diagrams depicting the structure of (a) the $\text{Au}_{13}$ core of the cluster. (b) the $\text{Au}_{13}$ core with 6 $-(\text{Au}_2\text{S}_3)-$ “staples” orientated around the 12 vertices. and (c) The $[\text{TOA}^+][\text{Au}_{25}(\text{SCH}_2\text{CH}_2\text{Ph})_{18}]$ complex (note, the real complex contains 2 $[\text{TOA}^+]$ ligands but has been omitted by the authors for clarity. Adapted from [280] .....	30



Figure 1-11. Transmission electron micrograph of gold particles encapsulated with a 10 nm tin dioxide layer. Adapted from [263].	31
Figure 1-12. The structure of the $[\text{HNi}_{24}\text{Pt}_{17}(\text{CO})_{25}(\mu\text{-CO})_{21}]^{5-}$ pentaanion. Pt atoms shown as orange spheres, Ni green, C grey and O red. Adapted from [288].	32
Figure 2-1. Schematic of a DC magnetron sputtering chamber.	40
Figure 2-2. Schematic of the core shell electron ejection process and X-ray generation by outer shell filling.	43
Figure 2-3. Schematic representation of the fabrication of discrete nanoscale capacitors and the charging process. (a) Close-packed latex spheres on silicon are prepared by spin-coating. (b) Close-packed spheres act as a mask so that gold deposited by evaporative deposition forms discrete, patterned structures on the silicon substrate. Gold also deposits on the latex spheres. (c) A metal oxide layer is deposited by RF magnetron sputtering. (d) A second layer of gold is deposited by evaporative deposition. (e) Removal of the latex spheres results in periodic nanostructured arrays of capacitive triangles. (f) Charging of the nanostructures is achieved by repeatedly scanning an electron beam (represented by yellow triangle and purple arrow) across the sample. Dark grey = Si substrate, Light grey = latex spheres, Orange = gold, Blue = metal oxide.	45
Figure 2-4. AFM image and line profile of calibration grating used for Atomic force microscope calibration.	48
Figure 2-5 AFM image and line profile of gold step used for film thickness monitor calibration.	49
Figure 3-1. (a) AFM image of periodic structures fabricated using NSL. Large bright regions indicate mask defects where spheres did not form continuous hcp orientations. (b) grey-scale intensity vs. time data used to estimate the capacitance of structures produced in (a). (c) SEM images of nanostructures imaged over time. The greyscale intensity data is extracted from these images in (b). Data adapted from [19].	53

Figure 3-2. Column graph showing the number of papers containing the topics “natural lithography”, “nanosphere lithography” and “colloidal lithography” between 1982 (first natural lithography paper published) and 2015. Data obtained from ISI Web of Knowledge (accessed 29<sup>th</sup> February 2016). .....55

Figure 3-3. Schematic representing the spin-coating process being used to fabricate ordered arrays of close packed spheres for NSL. (a) Schematic depicting a solution of monodisperse PS latex being spin-coated onto a silicon substrate. (b) Schematic representing ordered array of hexagonally close packed PS spheres on silicon. ....56

Figure 3-4. SEM micrographs of NSL masks used to investigate the effect of spin-coat volume on hcp ordering. Solutions were spin-coated onto silicon substrates with a “drop before spinning” method at 3600 RPM for 40s for mask formation. Subsequently, 20 nm of gold was deposited on the samples via evaporative deposition followed by thorough rinsing in dichloromethane (DCM). .....57

Figure 3-5. SEM micrographs of 200 nm latex sphere mixtures spin-coated onto silicon substrates with a (10 % w/v aqueous sphere solution) : (1:400 Triton-X : methanol) ratio of (a) 3:1 and (b) 2:1. Samples were prepared by spin-coating 20  $\mu$ L mixtures on 1 cm<sup>2</sup> silicon substrates at 3600 RPM for 40 s in a “drop before spinning” method.....59

Figure 3-6. SEM micrographs of 200 nm latex sphere mixtures spin-coated onto silicon substrates with a (10 % w/v aqueous sphere solution) : (1:400 Triton-X : methanol) ratio of (a) 1:1, (b) 1:1.5, (c) and (d) 1:2, (e) 1:2.5 and (f) 1:3. Following spin-coating 20 nm of gold was deposited onto samples via evaporative deposition. Masks were prepared by spin-coating 20  $\mu$ L mixtures on 1 cm<sup>2</sup> *p*-type silicon substrates at 3600 RPM for 40 s in a “drop before spinning” method. ....60

Figure 3-7. SEM micrographs of 200 nm latex sphere mixtures spin-coated onto silicon substrates with a (10 % w/v aqueous sphere solution) : (1:400 Triton-X : methanol) ratio of (a) 10:1, (b) 3.33:1, (c) 2.5:1, (d) 1:1.2, (f) 1:1.3, (g) 1:1.4, (h) 1:1.5, (i) 1:1.6, (j) 1:1.7, (k) 1:1.8, (l) 1:1.9, (m) 1:2, (n) 1:3.7 and (o) 1:4. (e) shows a low magnification image for areas that exhibit hcp regions. Following spin-coating 20 nm of gold was deposited on the samples via evaporative deposition and mask

removal was facilitated by 1 min sonication and subsequent thorough rinsing in DCM. Samples were prepared by spin-coating 20  $\mu\text{L}$  mixtures on 1  $\text{cm}^2$  *p*-type silicon substrates at 3600 RPM for 40 s in a “drop while spinning” method..... 62

Figure 3-8. SEM micrographs of 200 nm latex sphere mixtures spin-coated onto silicon substrates with a (10 % w/v aqueous sphere solution) : (1:400 Triton-X : methanol) ratio of (a) and (b) 3:1, (c) 4:1, (d) 5:1, (e) and (f) 6:1. Following spin-coating 20 nm of gold was deposited on the samples via evaporative deposition. Samples were prepared by spin-coating 20  $\mu\text{L}$  mixtures on 1  $\text{cm}^2$  *p*-type silicon substrates at 3600 RPM for 40 s in a “drop before spinning” method. .... 64

Figure 3-9. SEM micrographs of sphere mixtures spin-coated onto silicon substrates with a (10 % w/v aqueous sphere solution) : (1:400 Triton-X : methanol) ratio of 4:1. Size of the spheres are (a) and (b); 500 nm, (c) and (d); 900 nm, (e) and (f); 1500 nm. Following spin-coating 20 nm of gold was deposited on the samples via evaporative ((a), (b), (e) and (f) or sputter (c) and (d)) deposition. Mask removal (with the exception of (a) and (b)) was facilitated by 1 min sonication and subsequent thorough rinsing in DCM..... 66

Figure 3-10. (a) Scanning electron micrograph of NSL mask composed of an array of close-packed 1500 nm PS spheres sputter coated with 20 nm of gold. (b) Gold triangular structures that remain after mask removal by sonication and rinsing in dichloromethane. Green circles highlight sections of gold triangles that have been displaced from the array..... 67

Figure 3-11. SEM micrograph of a silicon substrate after the removal of a 1500 nm PS latex sphere NSL mask via tape stripping. Contact patches where spheres resided before removal are clearly visible..... 68

Figure 3-12. Schematic representing the experimental procedure used in the lift-off method. PS latex / surfactant mixtures are placed at the air-water interface of a petri dish and allowed to close pack via hydrophobic forces. A hydrophilic silicon substrate is then lifted through the floating film. .... 69

Figure 3-13. SEM micrographs of structures produced by the lift off process of 500 nm PS spheres, coated with 10 nm of gold (a) without and (b) with PS sphere removal. ....	69
Figure 3-14. SEM micrographs of (a) 1500 nm close packed PS spheres. Triangular nanostructures formed by sputter deposition (b) and evaporative deposition (c) of gold.....	71
Figure 3-15. SEM micrographs of gold nanostructures produced by (a) evaporative coating or sputter coating 20 nm gold films on NSL templates utilising 1500 nm PS latex sphere masks. Sputtering argon partial pressure and power supply conditions were (b) $6 \times 10^{-4}$ Torr, 0.017 A, 20 V, (c) $3 \times 10^{-4}$ Torr, 0.017 A, 20 V and (d) $3 \times 10^{-4}$ Torr, 0.020 A, 20 V.....	73
Figure 4-1. SEM micrograph of nanoscale capacitors fabricated NSL. Films consisting of gold (20 nm) / hafnia (20 nm) / gold (20 nm) layers were synthesised. 80	
Figure 4-2. (a) Schematic representing the nanostructures produced for charging experiments. (b) Scanning electron micrograph of a nanostructure fabricated by depositing 20 nm of gold / 20 nm of alumina / 20 nm of gold (deposition of top layer of gold was offset in this example by tilting the sample during the last deposition cycle in order to facilitate visualisation of the uppermost gold layer. Image parameters: accelerating voltage, 20 keV, working distance, 1.8 mm. (c) AFM image and section line profile overlay of 20 nm gold / 20 nm hafnia / 20 nm gold nanostructure (structure synthesised with a larger offset of bottom gold layer to aid film thickness measurements).....	81
Figure 4-3. Monte Carlo simulation results for an electron beam irradiating a gold (20 nm) / alumina (20 nm) / gold (20 nm) film on a silicon substrate with different accelerating voltages. (a); 2 keV, (b); 1 keV and (c); 0.3 keV. The trajectories of electrons that generate secondary and backscattered electrons are represented by blue and red lines respectively. Horizontal dashed lines represent material interfaces. (d) Schematic representing the interaction of a low accelerating voltage electron beam with fabricated nanoscale devices.....	82

Figure 4-4. SEM micrographs of nanoscale capacitors fabricated utilising NSL. Films consisting of gold (20 nm) / alumina (20 nm) / gold (20 nm) layers were synthesised. (a); image of six discrete structures. (b); image of an individual structure. (c); low accelerating voltage image of an array of structures at the beginning of the charging process. (d); low accelerating voltage image of the same array at the completion of the charging process. ....	83
Figure 4-5. SEM micrographs of a gold (20 nm) / alumina (20 nm) / gold (20 nm) nanosandwich array collected under a 0.3 keV accelerating voltage. Time data overlayed on the images is in s. ....	85
Figure 4-6. Plot of grey-scale intensity vs. time, for the charging of sixteen gold (20 nm) / alumina (20 nm) / gold (20 nm) nanosandwiches. Average grey-scale intensity of silicon substrate and an average value for the top gold triangular structures (blue and orange traces respectively) are also presented. ....	87
Figure 4-7. Schematic representation of the charge configuration of an individual gold (20 nm) / alumina (20 nm) / gold (20 nm) nanostructure at $t \sim 500$ s (a) and $\sim 1200$ s (b). Surface charges are displayed in white, electric field lines in red and electrons injected into the sample by the focused electron beam in yellow. ....	88
Figure 4-8. Graphs of mean grey-scale intensities vs. time for edge (red) and middle (blue) regions of the top gold layer of a single gold (20 nm) / alumina (20 nm) / gold (20 nm) structure ('Triangle #7'). ....	90
Figure 4-9. SEM micrographs of nanoscale capacitors fabricated utilising NSL. Films consisting of gold (20 nm) / silica (20 nm) / gold (20 nm) layers were synthesised. (a); image of six discrete structures. (b); image of an individual structure. Low accelerating voltage images of an array of structures at the beginning (c) and completion (d) of the charging process. ....	92
Figure 4-10. SEM micrographs of a gold (20 nm) / silica (20 nm) / gold (20 nm) nanosandwich array collected under a 0.3 keV accelerating voltage. Time data overlayed on the images is in s. ....	93

Figure 4-11. Plot of grey-scale intensity vs. time, for the charging of seventeen gold (20 nm) / silica (20 nm) gold (20 nm) nanosandwiches. Average grey-scale intensity of silicon substrate and an average value for the top gold triangular structures (blue and orange traces respectively) are also presented. ....94

Figure 4-12. SEM micrographs of nanoscale capacitors fabricated utilising NSL. Films consisting of gold (20 nm) / zinc oxide (20 nm) / gold (20 nm) layers were synthesised. (a); image of six discrete structures. (b); image of an individual structure. (c); low accelerating voltage image of an array of structures at the beginning of the charging process. (d); low accelerating voltage image of the same array at the completion of the charging process. ....95

Figure 4-13. SEM micrographs of a gold (20 nm) / zinc oxide (20 nm) / gold (20 nm) nanosandwich array collected under a 0.3 keV accelerating voltage. Time data overlayed on the images is in s. ....97

Figure 4-14. Plot of grey-scale intensity vs. time for the charging of sixteen gold (20 nm) / zinc oxide (20 nm) gold (20 nm) nanosandwiches. Average grey-scale intensity of silicon substrate and an average value for the top gold triangular structures (blue and orange traces respectively) are also included. ....98

Figure 4-15. SEM micrographs of nanoscale capacitors fabricated utilising NSL. Films consisting of gold (20 nm) / titania (20 nm) / gold (20 nm) layers were synthesised. (a); image of twenty discrete structures. (b); image of five discrete structures. (c); low accelerating voltage image of an array of structures at the beginning of the charging process. (d); low accelerating voltage image of the same array at the completion of the charging process. ....99

Figure 4-16. SEM micrographs of a gold (20 nm) / titania (20 nm) / gold (20 nm) nanosandwich array collected under a 0.3 keV accelerating voltage. Time data overlayed on the images is in s. ....101

Figure 4-17. Plot of grey-scale intensity vs. time for the charging of twenty gold (20 nm) / titania (20 nm) / gold (20 nm) nanosandwiches. Average grey-scale intensity of silicon substrate and an average value for the top gold triangular structures (blue and orange traces respectively) are also presented. ....102

Figure 4-18. SEM micrographs of nanoscale capacitors fabricated utilising NSL. Films consisting of gold (20 nm) / hafnia (20 nm) / gold (20 nm) layers were synthesised. (a); image of six discrete structures. (b); image of an individual structure. (c); low accelerating voltage image of an array of structures at the beginning of the charging process. (d); low accelerating voltage image of the same array at the completion of the charging process. .... 103

Figure 4-19. SEM micrographs of a gold (20 nm) / hafnia (20 nm) / gold (20 nm) nanosandwich array collected under a 0.3 keV accelerating voltage. Time data overlayed on the images is in s. .... 105

Figure 4-20. Plot of grey-scale intensity vs. time for the charging of fifteen gold (20 nm) / hafnia (20 nm) gold (20 nm) nanosandwiches. Average grey-scale intensity of silicon substrate and an average value for the top gold triangular structures (blue and orange traces respectively) are also presented. .... 106

Figure 4-21. SEM micrographs of nanoscale capacitors fabricated utilising NSL. Triangular structures consisting of gold (20 nm) layers were synthesised. (a); image of an individual structure. (b); high-magnification image of an individual structure. (c); low accelerating voltage image of an array of structures at the beginning of the charging process. (d); low accelerating voltage image of the same array at the completion of the charging process. .... 108

Figure 4-22. SEM micrographs of a gold (20 nm) array collected under a 0.3 keV accelerating voltage. Time data overlayed on the images is in s. .... 110

Figure 4-23. Plot of grey-scale intensity vs. time for the charging of seventeen gold (20 nm) nanostructures. Average grey-scale intensity of silicon substrate and an average value for the top gold triangular structures (blue and orange traces respectively) are also presented. .... 111

Figure 4-24. SEM micrographs of silicon substrate after NSL mask fabrication and subsequent removal without metal /metal oxide deposition. (a); low accelerating voltage image of substrate at the beginning of the electron beam irradiation process. (b); low accelerating voltage image of the same substrate at the completion of the electron beam irradiation process. .... 112

Figure 4-25. SEM micrographs of a silicon surface with latex spheres removed collected under a 0.3 keV accelerating voltage. Time data overlayed on the images is in s.....	113
Figure 4-26. Plot of grey-scale intensity vs. time for the charging of a silicon substrate. Average grey-scale intensity of silicon substrate is presented. ....	114
Figure 4-27. SEM micrographs of silicon substrate after NSL mask fabrication and subsequent removal without metal /metal oxide deposition. Subsequently, the substrate was left in a desiccator for three weeks. (a); low accelerating voltage image of substrate at the beginning of the electron beam irradiation process. (b); low accelerating voltage image of the same substrate at the completion of the electron beam irradiation process. ....	114
Figure 4-28. SEM micrographs of a silicon surface with latex spheres removed, imaged after three weeks. Imaging was performed under a 0.3 keV accelerating voltage. Time data overlayed on the images is in s. ....	116
Figure 4-29. Plot of grey-scale intensity vs. time for the charging of silicon comparator without deposited nanostructures left in desiccator conditions for three weeks after initial measurement.....	117
Figure 4-30. Graphs of grey-scale intensity vs. time for the silicon background for arrays of devices as well as unmodified silicon and gold-only arrays.....	118
Figure 4-31. SEM micrographs of a gold (20 nm) / silica (20 nm) / gold (20 nm) nanosandwich array collected under a 0.3 keV accelerating voltage. After extended imaging the electron beam was blanked for 1 h before resumption of imaging. Time data overlayed on the images is in s.....	119
Figure 4-32. Plot of grey-scale intensity vs. time for the charging of gold (20 nm) / silica (20 nm) / gold (20 nm) nanosandwiches with 1 h of no electron irradiation. Average grey-scale intensity of silicon substrate and an average value for the top gold triangular structures (blue and orange traces respectively) are also included. ....	120
Figure 4-33. SEM micrographs of nanoscale structures fabricated using NSL. Films consisting of (a); gold (20 nm) / hafnia (20 nm) / gold (20 nm), (b); gold (20	



nm) / zinc oxide (20 nm) / gold (20 nm), (c) and (d) gold (20 nm) / alumina (20 nm) / gold (20 nm) were deposited via sputter deposition. All structures failed to demonstrate charging characteristics under imaging with a low energy electron beam (d)..... 121

Figure 4-34. SEM micrographs of nanoscale structures fabricated utilising NSL. Films consisting of gold (20 nm) / zinc oxide (20 nm) / gold (20 nm) layers were deposited via evaporative (gold) and sputter (zinc oxide) deposition. After the removal of the mask by 1 min sonication and subsequent rinsing in DCM, samples were left in a sample tube filled with DCM overnight before removal and thorough rinsing again in DCM..... 122

Figure 4-35. SEM micrographs of a nanoscale structure fabricated utilising NSL. After the removal of the mask by 1 min sonication and subsequent rinsing in DCM, samples were annealed at 300°C for 3 hr under high vacuum conditions ( $\sim 10^{-7}$  Torr ( $1.3 \times 10^{-5}$  Pa)). Films consisting of gold (20 nm) / zinc oxide (20 nm) / gold (20 nm) were deposited via evaporative (gold) and sputter (metal oxide) deposition. .... 123

Figure 5-1. SEM micrograph of triangular pyramids and zinc oxide rings that result from the metal / metal oxide sputtering of gold (20 nm) followed by zinc oxide (10 nm) on a NSL mask fabricated with 1500 nm PS latex spheres. PS latex sphere mask has been removed. Image is acquired with a 0.57 keV potential (relatively low accelerating voltage) to maximise SE emission from the surface enhancing the contrast from the differences in zinc oxide morphology. .... 127

Figure 5-2. SEM micrograph of gold (20 nm) / zinc oxide (10 nm) / nano-structures..... 128

Figure 5-3. Schematic showing the procedure to prepare the new structures. (a) Spheres are deposited on silicon surface. (b) Gold is deposited on spheres and onto silicon through the inter-sphere voids. (c) Zinc oxide is deposited on gold spheres and nanostructures, however small amounts of zinc oxide are also deposited on the silicon substrate in between the nanostructures and the latex spheres. .... 128

Figure 5-4. SEM micrograph of the triangular pyramids fabricated by the deposition of 10 nm of zinc oxide through a 1500 nm PS latex sphere mask. .... 129

Figure 5-5. AFM image of gold (20 nm) / zinc oxide (10 nm) structures with corresponding line profile (red trace) of indicated section (white dashed line). ..... 130

Figure 5-6. Monte Carlo simulation results for a 3 keV electron beam irradiating a gold (20 nm) / zinc oxide (10 nm) film on a silicon substrate. The trajectories of electrons that generate secondary and backscattered electrons are represented by blue and red lines respectively. Coloured horizontal dashed lines represent material interfaces. .... 131

Figure 5-7. Scanning electron micrograph and energy-dispersive X-ray spectroscopy of gold (20 nm) / zinc oxide (10 nm) template. Performed with a 3.0 keV accelerating voltage (a) SEM micrograph of array sample, (b) colour map representing the different regions of the array (made from (a)), (c-g) X-ray spectra of the different regions of the sample..... 132

Figure 5-8. Schematic for the proposed mechanism for the formation of zinc oxide rings. The green circles are latex spheres, yellow indicates deposited gold, purple deposited zinc oxide and the red lines indicate deposited zinc oxide trajectory. .... 134

Figure 5-9. Proposed mechanism for the formation of the zinc oxide rings. Distribution of electric equipotentials (solid lines) and direction of field lines (vectors) for the case where the triangle has accumulated a negative potential relative to the silicon substrate (the latex sphere is treated as an insulator in this simulation). The drawing is to scale and uses the experimental AFM topography in the calculation. The zinc oxide is the blue phase. Modelling and image provided by Professor Michael Cortie..... 135

Figure 5-10. SEM micrographs of gold (20 nm) / zinc oxide (10 nm) deposited on (a) p-type (100) and (b) n-type (111) Silicon..... 137

Figure 5-11. (a) AFM data of arrays fabricated by deposition of platinum (20 nm) / zinc oxide (10 nm) through NSL masks with corresponding line profile (red trace) for the specified section (white dashed line). (b) SEM micrograph of the sample shown in panel (a). Green circle indicates a region of between two platinum triangles that are seen to be in physical contact..... 137

Figure 5-12. SEM micrographs of different regions of arrays produced from the re-emission of 10 nm zinc oxide films on platinum (20 nm) triangles. (a) Large grain boundary between hcp regions. (b) Area near the edge of a hcp region. .... 138

Figure 5-13. Results of modelling carried out to determine the resultant equipotential distribution from a point source charge (solid red circle) on a mathematical representation of a faraday cage composed of various wire thicknesses. Figure reproduced from [439]. .... 139

Figure 5-14. SEM micrographs of arrays produced from the re-emission of 10 nm zinc oxide films on a continuous gold film (100 nm) (a) and hafnia (20 nm) triangular structures (b). .... 140

Figure 5-15. SEM micrographs of arrays produced from the re-emission of 10 nm zinc oxide films on structures consisting of connected silver (20 nm) (a) and connected gold (20 nm) triangular structures (b). Gold deposition parameters: Argon partial pressure  $3 \times 10^{-4}$  Torr ( $4 \times 10^{-2}$  Pa). Power supply settings (0.030 A, 20 V). .... 141

Figure 5-16. SEM micrographs of arrays of fabricated triangular structures by deposition of zinc oxide from zinc nitrate / hexamine solutions onto templates with various compositions. Samples were all incubated for 3 hrs at 90°C in aqueous solution containing equimolar concentrations of zinc nitrate and hexamine (10 mM). (a) Gold (20 nm), green circles indicate zinc oxide material. (b) Zinc oxide (10 nm). (c) Gold (20 nm) / zinc oxide (10 nm). (d) Gold (20 nm) / zinc oxide (20 nm) / gold (20 nm). .... 143

Figure 5-17. SEM micrographs of arrays fabricated by deposition of zinc oxide from zinc nitrate solutions of various concentrations onto templates consisting of gold (20 nm) / zinc oxide (20 nm) / gold (20 nm) and incubated at 90°C for 3hrs. Concentrations of zinc nitrate / hexamine are; (a) 0.1 mM. (b) 1 mM. (c) 10 mM. (d) 0.1 M. .... 145

Figure 5-18. SEM micrographs of arrays fabricated by deposition of zinc oxide from zinc nitrate solutions of various incubation times onto templates consisting of gold (20 nm) / zinc oxide (20 nm) / gold (20 nm) nanostructures. 10 mM

concentrations of zinc nitrate / hexamine were incubated at 90°C for; (a) 15 min. (b) 1 hr. (c) 2 hrs. (d) 3 hrs. .... 146

Figure 5-19. Scanning electron micrographs of 20 nm gold / 10 nm zinc oxide / 20 nm gold nano-sandwiches grown hydrothermally in 10mM ZnNO<sub>3</sub> and hexamine solutions for 3h. Incubation temperatures were varied from (a) 80°C, (b) 90°C and (c) 150°C. These images show significant change in the amount and diameter of zinc oxide nanorods produced. .... 147

Figure 5-20. Low (a) and high (b) magnification scanning electron micrographs show that at elevated temperatures (150°C) of growth solution, zinc oxide exhibits hexagonally-faceted tubes with ~200 nm diameter and ~1-2 µm length..... 148

Figure 5-21. (a) Schematic illustration showing the apparatus used to apply bias during zinc oxide growth. (b)-(d) SEM micrographs of arrays fabricated by growth of zinc oxide from zinc nitrate solution on templates consisting of gold (20 nm) / zinc oxide (20 nm) / gold (20 nm) at 90°C for 3hrs with various applied potentials; (b) - 0.5V. (c) 0V. (d) +0.5V potentials. .... 148

Figure 5-22. SEM micrographs of (a) zinc oxide ring and (d) solution precipitate with their corresponding cathodoluminescence (CL) images ((b) and (e) respectively). Cathodoluminescence (CL) spectra of the ring (c) and precipitate (f). Green circles indicate regions where spectra were acquired. Spectra and images acquired by Professor Matthew Phillips. .... 150

Figure 6-1. SEM micrograph of structures produced with 900 nm PS spheres coated with 20 nm of gold following substrate sonication in dichloromethane for 5 min. .... 154

Figure 6-2. Attachment of a gold particle to a grounded dielectric for SEM investigation into the capacitive properties of the particle / dielectric / metal system. .... 156

Figure 6-3. SEM micrographs of citrate stabilised gold nanoparticles attached to a silicon substrate via a silane / thiol thin film both before (a) and after (b) sintering. Particles were sintered by vacuum annealing at 200°C for three hours..... 157

Figure 6-4. SEM micrograph of 20 nm gold / 20 nm hafnia / 20 nm gold nanostructured thin films deposited on a 1500 nm PS sphere (gold layers have been offset for clarity). .....	158
Figure 6-5. SEM micrograph of continuous structures fabricated by deposition of platinum (20 nm) / zinc oxide (10 nm) through a NSL mask composed of hcp 1500 nm PS latex spheres. ....	159
Figure 7-1. Photographic image of the sample holder configuration of a SDT 2960 with simultaneous TGA-DSC. The sample under analysis is in the left crucible, the right crucible is a reference used for DSC measurements .....	163
Figure 7-2. Top: MS data for gold nanoparticles heated in air/argon at $2^{\circ}\text{C}.\text{min}^{-1}$ . The possible identities of five significant fragments are indicated. Data for nitrogen and argon are not shown. Bottom: TGA and DSC curves. Data are slightly asymmetrical during sinter ignition because the rapid rate of heat release temporarily increases the samples temperature above the furnace setpoint. ....	167
Figure 7-3. MS data collected for gold nanoparticles heated in a vacuum ( $10^{-4} - 10^{-6}$ Pa).....	167
Figure 7-4. Graphs of XPS data showing intensity ratios for (a) $\text{S}_{2p} / \text{Au}_{4f}$ and (b) $\text{C}_{1s} / \text{Au}_{4f}$ , measured on 1-butanethiol-stabilised gold nanoparticles as a function of annealing temperature and surrounding environment.....	169
Figure 7-5. Peak shape analysis of the $\text{S}_{2p}$ envelope for (a) pristine nanoparticles, (b) nanoparticles heated in air at $155^{\circ}\text{C}$ , (c) nanoparticles in air at $260^{\circ}\text{C}$ , and (d) nanoparticles heated in ultra-high vacuum at $271^{\circ}\text{C}$ . ....	170

## List of Tables

Table 1-1. Metal Oxide materials for nanoscale capacitor applications. ....	15
Table 1-2. Carbon nanotubes for nanoscale capacitor applications .....	18
Table 1-3. Carbon nanotube composites for nanoscale capacitor applications. ....	20
Table 1-4. Capacitive data for graphene based materials. ....	22
Table 1-5. Graphene composites.....	23
Table 1-6. Electrode composition of the different composite polymer supercapacitors. Adapted from [249].....	26
Table 1-7. Summary of the literature utilising conductive polymers for nanoscale capacitor applications.....	27
Table 1-8. Capacitance of cylindrical and spherical MCCs and calculated relative permittivities' of co-ordinated carbon monoxide. ( $\epsilon_{\text{CO monolayer}}$ ). Adapted from [290]. Farad per gram values have been inserted for ease of comparison to other materials.	33
Table 3-1. Measured areas of gold structures using different gold deposition conditions.....	74
Table 4-1. Properties of interest for metal oxides investigated to synthesise nanoscale capacitors.....	79
Table 4-2. Calculated time constants and capacitance.....	107

## Abbreviations

$\gamma$ - PGA = Poly- $\gamma$ -Glutamic Acid  
AC = Activated Carbon  
AES = Auger Electron Spectroscopy  
AFM = Atomic Force Microscopy  
AMU = Atomic Mass Units  
AR NSL = Angle-Resolved NanoSphere Lithography  
CAFM = Conducting Atomic Force Microscopy  
CL = Cathodoluminescence  
DSC = Differential Scanning Calorimetry  
CV curve = Cathodic potential or Cyclic Voltammetry curve  
CVD = Chemical Vapour Deposition  
CVP = Capacitance Voltage Profile  
DC = Direct Current  
DCM = Dichloromethane  
DNA = Deoxyribonucleic Acid  
DPV = Differential Pulse Voltammetry  
DRAM = Dynamic Random Access Memory  
DWCNT = Double-Walled Carbon Nanotubes  
EDS = Energy-Dispersive X-ray Spectroscopy  
 $E_F$  = Fermi level  
ESEM = Environmental Scanning Electron Microscopy  
fcc = Face-centred cubic  
GO = Graphene Oxide  
hcp = Hexagonal close-packing  
HOMO = Highest Occupied Molecular Orbital  
HOPG = Highly Ordered/Orientated Pyrolytic Graphite  
HV = High Vacuum  
IC = Integrated Circuit  
IR = Inner Region  
IUPAC = International Union of Pure and Applied Chemistry  
IV = Current Voltage

LUMO = Lowest Unoccupied Molecular Orbital  
 LSV = Linear Sweep Voltammetry  
 MCC = Metal Carbonyl Cluster  
 MPC = Monolayer Protected Cluster  
 MS = Mass Spectrometry  
 MWCNT = Multi-Walled Carbon NanoTube  
 n-type = Negative-type  
 NMR = Nuclear Magnetic Resonance  
 NSL = NanoSphere Lithography  
 p-type = Positive-type  
 PANi = Polyaniline  
 PEDOT = Poly (3,4-ethylenedioxythiophene)  
 pFPT = Poly(3-(4-fluorophenyl)thiophene)  
 pMeT = Poly(3-methylphenylthiophene)  
 PS = Polystyrene  
 pTh = Poly(thiophene)  
 PVD = Physical Vapour Deposition  
 QCM = Quartz Crystal Microbalance  
 RF = Radio Frequency  
 RPM = Revolutions Per Minute  
 SAM = Self-Assembled Monolayer  
 SE = Secondary Electron  
 SDS = Sodium Dodecyl Sulphate  
 SEM = Scanning Electron Microscopy  
 SERS = Surface Enhanced Raman Spectroscopy  
 STM = Scanning Tunnelling Microscopy  
 STS = Scanning Tunnelling Spectroscopy  
 Surfactant = Surface active agent  
 SWCNT = Single-Walled Carbon NanoTube  
 T<sub>A</sub> = Annealing Temperature  
 TEM = Transmission Electron Microscopy  
 TFT = Thin Film Transistor  
 TGA = Thermogravimetric Analysis



TLC = Thin Layer Chromatography

T<sub>M</sub> = Melting Temperature

T<sub>S</sub> = Substrate Temperature

UHV = Ultra High Vacuum

UTS = University of Technology, Sydney

UV = Ultraviolet

XPS = X-ray Photoelectron Spectroscopy

ZSR = Zero State Response

---

## Publications and Conference Proceedings Arising From This Work

1. Coutts. M. J.; Zareie. H. M.; Cortie. M. B.; Phillips. M. R.; Wuhler. R.; McDonagh. A. M., *Exploiting Zinc Oxide Re-emission to Fabricate Periodic Arrays*. ACS Applied Materials & Interfaces. 2010 **2**(6): p. 1774-1779.
2. Cortie. M. B.; Coutts. M.J.; Ton-That. C.; Dowd. A.; Keast. V. J.; McDonagh. A. M., *On the Coalescence of Nanoparticulate Gold Sinter Ink*. J. Phys. Chem. C. 2013 **117**(21): p. 11377–11384.
3. Coutts. M. J.; Zareie. H. M.; Cortie. M. B.; McDonagh. A. M., *Charging of gold/ metal oxide/ gold nanocapacitors in a scanning electron microscope*. Nanotechnology. 2014 **25**(15): p. 155703.
4. Coutts. M. J.; Zareie. H. M.; Cortie. M. B.; Phillips. M. R.; Wuhler. R.; McDonagh. A. M., *Patterning nanostructures for ZnO nanorod growth*. *International Conference on Nanoscience and Nanotechnology (ICONN 2010)*. 2010. Sydney, Australia.
5. Riessen. D.; Coutts. M. J.; Zareie. H. M.; McDonagh. A.M., *Ruthenium phthalocyanine thin films on gold*. *International Conference on Nanoscience and Nanotechnology (ICONN 2010)*. 2010. Sydney, Australia.
6. Coutts. M. J.; Zareie. H. M.; Cortie. M. B.; Phillips. M. R.; Wuhler. R.; McDonagh. A. M., *Solution Growth of Zinc Oxide on Templates Fabricated by Re-emission of Sputtered Materials*. *Inaugural One-day Student Symposium in Inorganic Chemistry*. 2011. School of Chemistry, The University of Sydney, Australia.

## Abstract

Nanosphere lithography was used to synthesise nanoscale capacitors as well as arrays of zinc oxide nanostructures. Close-packed polystyrene nanospheres were used as masks and periodic arrays of metals / metal oxides were deposited through the inter-sphere voids onto substrates. The technique was optimised to produce hexagonally close-packed arrays of polystyrene spheres for a range of sphere sizes (200-1500 nm). Nanoscale capacitors were synthesised via evaporative and sputter deposition to produce structures consisting of gold / metal oxide / gold layers on a silicon substrate. A range of metal oxides were investigated including alumina, silica, zinc oxide, titania and hafnia. A significant development reported here involves the charging of these devices and their characterisation using scanning electron microscopy techniques. These methods enable the measurement of the charging time constants of materials in a non-destructive fashion without the requirement to connect wires or contacts. Nanostructures fabricated using zinc oxide as a dielectric material produced rings of zinc oxide nanostructures on the silicon substrate and a mechanism for the ring formation is proposed here. The resultant structures were used as templates to seed the hydrothermal growth of zinc oxide nanostructures. Arrays of zinc oxide nanostructures were also produced using techniques that enable control over the position and amount of growth.